Original papers
Materials for energy and environment, next-generation photovoltaics, and green technologies

УДК 66.081.3 DOI: 10.17277/jamt-2025-10-02-154-166

Sorption dynamics of organic dyes from aqueous solutions using activated carbon derived from peach modified with carbon nanotubes

© Ali H. K. Kadum[a], Irina V. Burakova [a]✉, Dmitry A. Badin[a], Sofya O. Rybakova[a], Alexey N. Timirgaliev[a], Vladimir O. Yarkin[a], Tatyana S. Kuznetsova[a], Tatyana P. Dyachkova[a], Alexander E. Burakov[a]

[a] *Tambov State Technical University, Bld. 2, 106/5, Sovetskaya St., Tambov, 392000, Russian Federation*

✉ iv.burakova@mail.ru

Abstract: This study synthesized nanocomposite activated carbon (AC) from plant raw materials (peach production waste), modified with carbon nanotubes (CNTs). The first stage in obtaining all samples involved hydrothermal carbonization (HTC) of peach pomace in an aqueous environment with the addition of a specific amount of CNTs, after which the biomass was gradually carbonized and activated using an alkali (KOH) in an inert atmosphere. The aim of the study was to evaluate the effect of CNTs on the structure and physicochemical and functional properties of the nanocomposite AC. It was established that the carbon obtained from the initial mixture containing 0.05 wt. % CNTs showed a specific surface area according to the BET model of 2876 $m^2 \cdot g^{-1}$ and a total pore volume of 1.643 $cm^3 \cdot g^{-1}$. It is presumed that the interaction of the biomass with the nanotubes occurs at sites on the surfaces of the samples after HTC, where functional groups are located. The sample with 0.05 wt. % CNTs exhibited minimal I_D/I_G and d_{100} values, indicating a higher order of the carbon structure. For all carbons, the sorption capacity relative to synthetic dyes – malachite green (MG) and Congo red (CR) – was determined. A general correlation was found between the changes in the I_D/I_G and d_{100} values and the activity of the AC samples. The AC with 0.05 wt. % CNTs demonstrated the highest capacity for both dyes in static mode: 2987 $mg \cdot g^{-1}$ for MG and 1201 $mg \cdot g^{-1}$ for CR, respectively. For this particular sample, an assessment of the sorption kinetics was conducted.

Keywords: activated carbon; biochar; carbon nanotubes; peach processing waste; synthetic dyes; Congo red; malachite green; adsorption dynamics; kinetics.

For citation: Kadum AHK, Burakova IV, Badin DA, Rybakova SO, Timirgaliev AN, Yarkin VO, Kuznetsova TS, Dyachkova TP, Burakov AE. Sorption dynamics of organic dyes from aqueous solutions using activated carbon derived from peach modified with carbon nanotubes. *Journal of Advanced Materials and Technologies*. 2025;10(2):154-166. DOI: 10.17277/jamt-2025-10-02-154-166

Динамика сорбции органических красителей из водных растворов активированным углем из персика, модифицированного углеродными нанотрубками

© А. Х. К. Кадум[a], И. В. Буракова[a]✉, Д. А. Бадин[a], С. О. Рыбакова[a], А. Н. Тимиргалиев[a], В. О. Яркин[a], Т. С. Кузнецова[a], Т. П. Дьячкова[a], А. Е. Бураков[a]

[a] *Тамбовский государственный технический университет, ул. Советская, 106/5, пом. 2, Тамбов, 392000, Российская Федерация*

✉ iv.burakova@mail.ru

Аннотация: В работе синтезировали нанокомпозиционный активированный уголь (АУ) из растительного сырья (отходов производства персика), модифицированного углеродными нанотрубками (УНТ). Первой стадией получения всех образцов была гидротермальная карбонизация (ГТК) персиковых выжимок в водной среде

с добавлением определенного количества УНТ, после чего биомассу поэтапно карбонизировали и активировали с помощью щелочи (КОН) в инертной среде. Цель работы – оценка влияния УНТ на структуру и физико-химические и функциональные свойства нанокомпозиционного АУ. Установлено, что уголь, полученный из исходной смеси, содержащей 0,05 мас. % УНТ, показывает величину удельной поверхности по модели БЭТ, равную 2876 м^2/г, и общий объем пор – 1,643 см^3/г. Предположительно, взаимодействие биомассы с нанотрубками происходит на участках поверхности образцов после ГТК, где расположены функциональные группы. Образец с 0,05 мас. % УНТ показывает минимальные значения I_D/I_G и d_{100}, что говорит о более высокой упорядоченности углеродной структуры. Для всех углей определяли сорбционную способность по отношению к синтетическим красителям – малахитовый зеленый (МЗ) и конго красный (КК). Обнаружена общая корреляция характера изменения показателей I_D/I_G и d_{100} с активностью образцов АУ. Наибольшую емкость по обоим красителям в статическом режиме показал АУ с 0,05 мас. % УНТ: 2987 и 1201 мг/г для МЗ и КК соответственно. Для указанного образца проведена оценка кинетики сорбции в динамическом режиме. По результатам экспериментальных и теоретических исследований определены такие важные показатели поглощения, как константы скорости сорбции и коэффициенты диффузии.

Ключевые слова: активированный уголь; биоуголь; углеродные нанотрубки; отходы переработки персика; синтетические красители; конго красный; малахитовый зеленый; динамика адсорбции; кинетика.

Для цитирования: Kadum AHK, Burakova IV, Badin DA, Rybakova SO, Timirgaliev AN, Yarkin VO, Kuznetsova TS, Dyachkova TP, Burakov AE. Sorption dynamics of organic dyes from aqueous solutions using activated carbon derived from peach modified with carbon nanotubes. *Journal of Advanced Materials and Technologies*. 2025;10(2):154-166. DOI: 10.17277/jamt-2025-10-02-154-166

1. Introduction

Global consumption of clean freshwater is increasing annually. However, its quality is noticeably declining. This is partly related to the problem of discharging untreated wastewater [1, 2]. More than 100,000 types of synthetic dyes are used in the textile, paint, paper, leather, and printing industries [3]. The discharge of wastewater from industrial enterprises leads to the accumulation of pollutants and has a negative impact on the environment [4, 5]. Malachite green (MG) is a common organic cationic dye used in chemical processes, the textile industry, as a medical disinfectant, and so on. Congo red (CR) is an azo dye, an acid-base indicator, and is used in histology and microscopic studies for staining fungal cell walls. Furthermore, adsorption is one of the most effective methods used for the removal of MG and CR [6, 7].

The choice of adsorbent is fundamental to the successful development, effectiveness, and implementation of the adsorption process. Activated carbon from plant material can compete with traditional coals due to its exceptional properties: high porosity, large surface area, and the presence of functional groups. Various methods of producing biochar are known, including hydrothermal carbonization (HTC), pyrolysis, and gasification [8, 9].

To enhance the adsorption capacity of biochar, modification of target waste is carried out to create active centers (functional groups) on its surface, which can effectively retain dyes under suitable conditions. Various methods of modification are known, including the use of acids, bases, surfactants, esterification, and the process of grafted copolymerization, resulting in the formation of different functional groups on the material's surface (hydroxyl, carboxylate, amide, amino, and ester groups). Waste from bananas, coconuts, apricots, peaches, etc., can be used as precursors for biochar production for wastewater treatment [10–12]. Peaches are consumed in nearly all parts of the world due to their unique flavor and aroma. The peach processing industry discards many parts of the fruit, including the pit and skin, referred to as "peach waste," which is rich in hemicellulose, lignin, and cellulose compounds, making these products valuable for the production of effective biochar [13].

The authors [12] synthesized biochar from the cladodes of the cactus Opuntia ficus-indica. Modification of the biochar using NaOH resulted in increased surface basicity. The maximum adsorption capacities based on the Langmuir model were found to be 1341, 49, and 44 mg·g^{-1} for MG, Cu^{2+} and Ni^{2+}, respectively.

The sorption capacity of biochar derived from date palm leaves [14] reached values of 334 mg·g^{-1} for MG. In the study [15], biochar obtained from banana peels was functionalized using microwave pyrolysis. It was established that the maximum adsorption capacity for MG reached 2297.83 mg·g^{-1} with a contact time of 120 min. The mechanism of dye adsorption for MG included hydrophobic interactions, the formation of hydrogen bonds, π-π interactions, and ion exchange.

The adsorption of Congo red (CR) was conducted using activated biochar from *Haematoxylum*

campechianum waste obtained through pyrolysis. The maximum adsorption capacity, determined using the Langmuir adsorption isotherm model, was found to be 114.8 $mg \cdot g^{-1}$ at 300.15 K, pH = 5.4, and an activated biochar dose of 1.0 $g \cdot L^{-1}$ [16]. Biochar from *Medulla Tetrapanacis* modified with K_2CO_3showed an adsorption capacity for CR of 584.17 $mg \cdot g^{-1}$ [17]. The adsorption capacity of the biochar from rice husks for CR amounted to 42.918 $mg \cdot g^{-1}$, with equilibrium adsorption occurring after 120 min. The process of CR adsorption on biochar took place through physical adsorption and chemisorption, involving hydrogen bonds, electrostatic interactions, and π-π interactions [18].

Another method for enhancing the sorption activity of biochars is the creation of composites with carbon structures (such as carbon nanotubes (CNTs), graphene, etc.), metal oxides, and others [19, 20]. A method has been developed for obtaining CNT-biochar nanocomposites using a surfactant derived from hickory chips and sugarcane bagasse [21]. In one study [22], biochar was synthesized from potato peeling waste (utilizing various activation technologies) followed by modification with CNTs.

The objective of this work is to study the organic dyes (MG and CR) adsorption dynamics on a nanocomposite material – activated carbon (AC) derived from peach pomace, modified with CNTs. To achieve the research goal, samples of composite biochars with varying mass percentages of CNTs were synthesized, their physicochemical properties were determined, and the kinetics of malachite green sorption in a dynamic mode were assessed.

2. Methods and Materials

2.1. Preparation of activated carbon modified with carbon nanotubes

Biochar was obtained through HTC in an aqueous environment from biomass generated from peach pomace, which was first dried and ground. The carbon nanotubes "Taunit-M" (LLC "NanoTechCenter", Tambov) were added in dry form (0.01, 0.05, 0.1, 0.5, 1 wt. %) to the powdered peach material, and the resulting mixture was further mechanically ground. The dispersed bulk material was placed in a stainless steel autoclave, and distilled water was added. The mass ratio of "bulk material : water" was 1 : 3. The mixture was processed in the autoclave at a temperature of 180°C for 12 hours. The obtained HTC biochar was filtered and washed with water to remove by-products of the reaction and dried to a constant residual mass at 90 °C. The material was then subjected to thermal carbonization at 150, 350, and 700 °C (for 1 hour at each temperature) in an inert argon environment (with a flow rate of 1.4 $L \cdot min^{-1}$). To obtain activated carbon, the carbonized samples were mixed with an alkali (KOH) in a mass ratio of 1:6, then treated in an argon atmosphere at 400 and 750 °C (for 1 hour at each temperature). The resulting material was washed with distilled water until a neutral pH (~7) was reached. It was then soaked in concentrated hydrochloric acid for 24 hours. Afterward, it was washed again until a neutral pH was achieved. The washed material was dried at 90 °C until a constant mass was obtained.

The obtained experimental samples of composite activated carbon were stored in airtight plastic containers.

2.2. Adsorption test

2.2.1. Static conditions

To preliminarily assess the sorption capacity of the developed materials toward organic dyes MG and CR, studies were conducted under limited-volume conditions with the following fixed parameters: initial dye model solution concentration – 1500 $mg \cdot L^{-1}$, pH = 6, sorbent weight – 0.01 g, contact time – 30 min. The optical density of the synthetic dye solutions was measured using a PE-5400V spectrophotometer (Ekros, St. Petersburg, Russia) at wavelengths λ(MG) = 810 nm and λ(CR) = 625 nm.

2.2.2. Dynamic conditions

Kinetic studies under dynamic conditions were carried out using an experimental setup (Fig. 1). A 100 mL stock solution of MG and CR with a concentration of 1500 $mg \cdot L^{-1}$ was delivered by a peristaltic pump (*3*) into a sorption cell (*1*) containing the sorbent (mass 0.03 g) and circulated back to the original reservoir (*R*). A parallel circuit was used to deliver the solution to a cuvette located in the spectrophotometer (*2*).

2.3. Analytical methods

The morphology of the materials was examined using scanning electron microscopy (SEM) with a TESCAN Vega III microscope (Czech Republic).

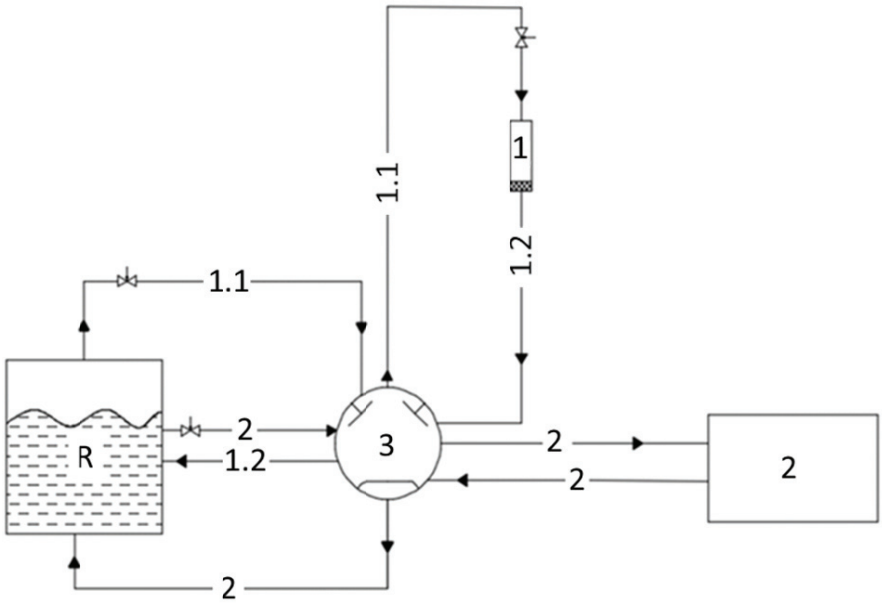

Fig. 1. Laboratory setup for dynamic sorption
(*R* – reservoir with the initial solution; *1* – sorption cell; *2* – spectrophotometer, *3* – peristaltic pump)

To qualitatively identify functional groups, FTIR spectra of the samples were recorded in attenuated total reflectance (ATR) mode using a Jasco FT/IR 6700 spectrometer (Jasco International Co., Ltd., Japan) in the wavenumber range of 500 to 4000 cm^{-1}. Structural features of the samples were determined based on Raman spectra, recorded with a DXR Raman Microscope (Thermo Scientific Instruments Group, Waltham, USA) using a laser excitation wavelength of $\lambda = 532$ nm. The phase composition of the materials was determined from X-ray diffraction (XRD) patterns obtained using a Thermo Scientific ARL Equinox 1000 diffractometer (TechTrend Science Co., Ltd., Taiwan).

To evaluate the thermal stability of the samples, simultaneous thermal analysis was performed – recording thermogravimetric (TG) curves and differential scanning calorimetry (DSC) curves simultaneously – using a NETZSCH STA 449 F3 Jupiter instrument (NETZSCH-Feinmahltechnik GmbH, Selb, Germany) under an air atmosphere with a heating rate of 10 $K \cdot min^{-1}$. The specific surface area and porous structure parameters were determined using a high-precision surface area and pore size analyzer TOP 200 (Altamira Instruments, USA). The specific surface area (S_{BET}) was calculated using the Brunauer–Emmett–Teller (BET) theory, and the total pore volume (V_{total}) was determined by the Barrett–Joyner–Halenda (BJH) method.

3. Results and Discussion

3.1. Evaluation of physicochemical properties

SEM-images of the biochars (Fig. 2*a*–*e*) show that all materials, regardless of treatment method, possess a rough, irregular, and variably porous structure. The morphology of the samples subjected to HTC treatment (Fig. 2*a*) is mainly represented by elongated grains (fibers) and microspheres. It was found that the introduction of CNTs during the hydrothermal carbonization stage results in a reduction in the diameter of the microspheres – from a size range of 200–250 nm to 100–200 nm (for HTC biochar modified with CNTs).

The modified HTC biochar (Fig. 2*b*, *c*) contains CNTs and catalyst particles with an average diameter of approximately 35 nm. According to the obtained images, the nanotubes are uniformly distributed within the carbon matrix derived from peach biomass and are directly encapsulated in the biochar microspheres. The sample of activated carbon modified with CNTs is characterized by inclusions up to 10 nm in diameter and the presence of bridges between the material grains. It is presumed that during the alkaline activation process, partial destruction of the CNT graphene structure occurred, resulting in the formation of connecting "bridges" between granules and an increase in surface defects due to the formation of grooves.

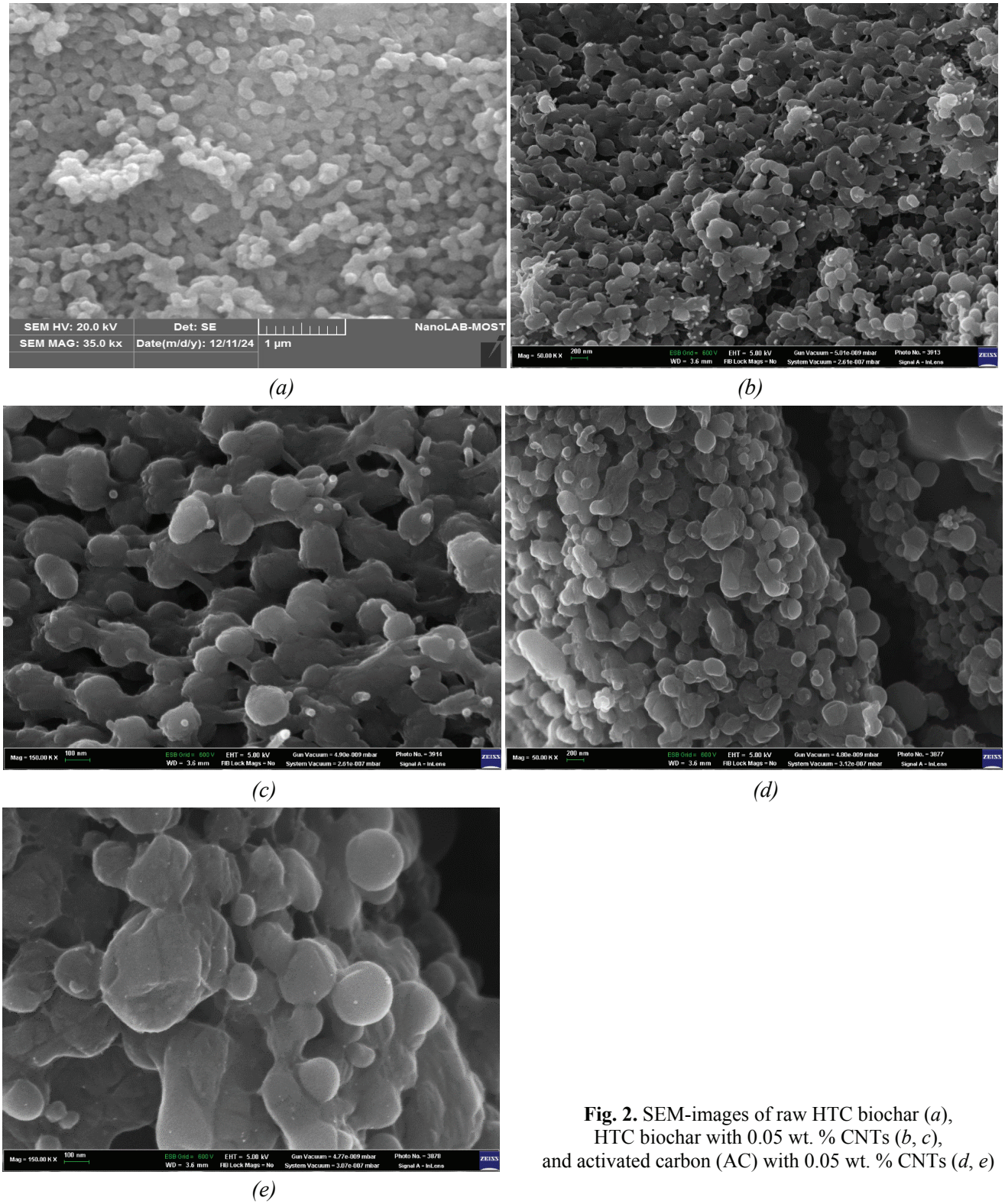

Fig. 2. SEM-images of raw HTC biochar (*a*), HTC biochar with 0.05 wt. % CNTs (*b*, *c*), and activated carbon (AC) with 0.05 wt. % CNTs (*d*, *e*)

Thus, the incorporation of CNTs into the biochar, regardless of the processing stage, led to changes in the surface morphology and grain size of the structural elements of the biochar. This suggests the formation of a more favorable porous architecture in the activated carbon for the removal of toxic pollutants from aqueous media.

To assess material changes under different processing conditions, IR-spectra were analyzed for the following samples: the original (HTC) and modified (HTC/CNT_0.01 et al.) materials after hydrothermal carbonization; the original carbonized coal (CC) and modified (CC/CNT_0.01 et al.) after thermal carbonization; and the original activated

carbon (AC) and modified (AC/CNT_0.01 et al.) after alkaline activation.

The IR-spectrum of the material obtained via HTC treatment of the raw material (without CNTs) (Fig. 3*a*) shows characteristic peaks attributed to:

– Stretching vibrations of O–H bonds in hydroxyl groups and/or water molecules (broad peak centered at 3423 cm^{-1});

– Asymmetric (2957 and 2922 cm^{-1}) and symmetric (2865 cm^{-1}) stretching vibrations of C–H bonds in alkyl groups;

– Stretching vibrations of C=O bonds in carboxyl groups (1710 cm^{-1}) and in carbonyl groups conjugated with two aromatic rings (1627 cm^{-1});

– Various vibration modes of oxygen-containing groups in cellulose fragments (group of peaks within the broad band of 1000–1500 cm^{-1}).

The addition of CNTs to the biomaterial does not qualitatively alter the chemical composition of the HTC products. A slight decrease in the intensity of all absorption bands is observed, which may be due to the chemical inertness of CNTs.

During carbonization (Fig. 3*b*), thermal decomposition removes most of the oxygen-containing functional groups. As a result, only the peaks at 3423 and 1627 cm^{-1} remain relatively intense in the IR-spectra. The former is likely due to adsorbed moisture, and the latter to the relatively high stability of the carbonyl bond conjugated with two aromatic rings. The intensities of peaks indicating the presence of alkyl groups and cellulose fragments are significantly lower compared to the spectra of HTC-treated samples. There is no qualitative difference in the composition of CNT-modified materials at this stage.

After alkaline activation (Fig. 3*c*), no significant changes are observed in the IR-spectra of the samples. However, it should be noted that the activated sample with the highest CNTs content has the most "depleted" composition, as its IR spectrum lacks peaks corresponding to alkyl and oxygen-containing groups in the 1000–1500 cm^{-1} region.

Based on scanning electron microscopy data, it can be assumed that the bonding between the nanotubes and the biomass-derived matrix during composite formation occurs at the sites originally occupied by functional groups. This likely explains the observed changes in the IR spectral characteristics.

All of the analyzed samples exhibit prominent *D* (~1350 cm^{-1}) and *G* (~1590 cm^{-1}) bands in their Raman spectra. The intensity ratio of these peaks (I_D/I_G) is commonly used to assess the degree of graphitization in carbon materials, where a higher I_D/I_G value indicates a greater level of structural disorder or defects in the sample [23, 24].

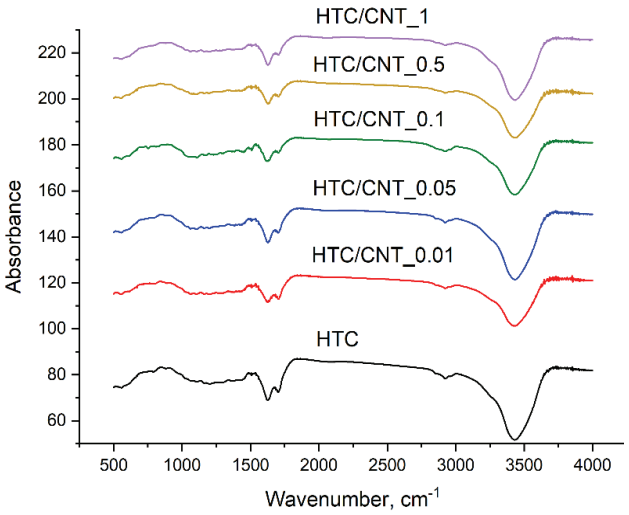

(a)

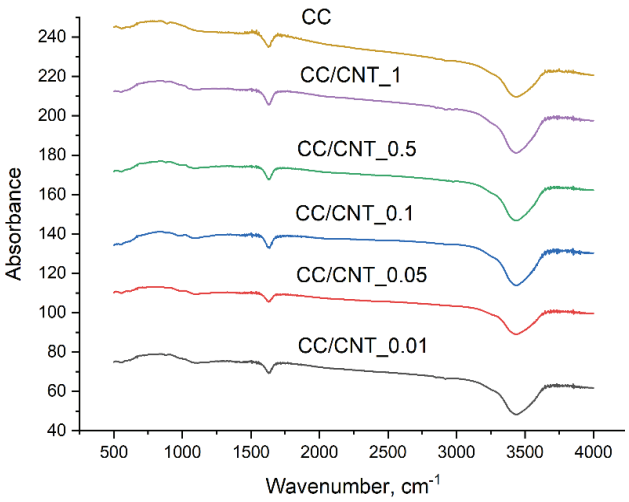

(b)

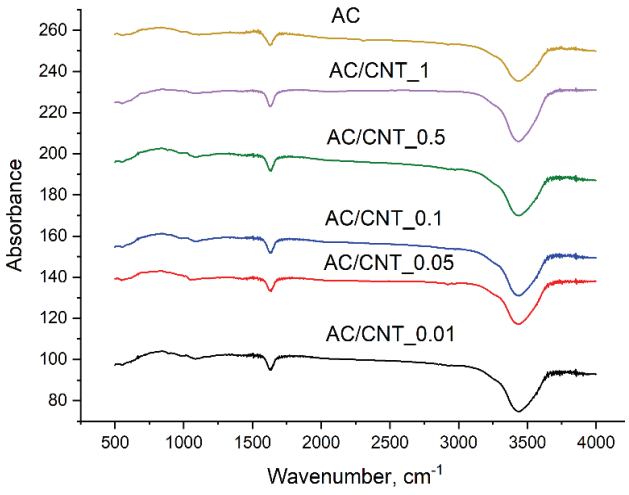

(c)

Fig. 3. IR-spectra of carbon samples: (*a*) after HTC; (*b*) after carbonization; (*c*) after alkaline activation

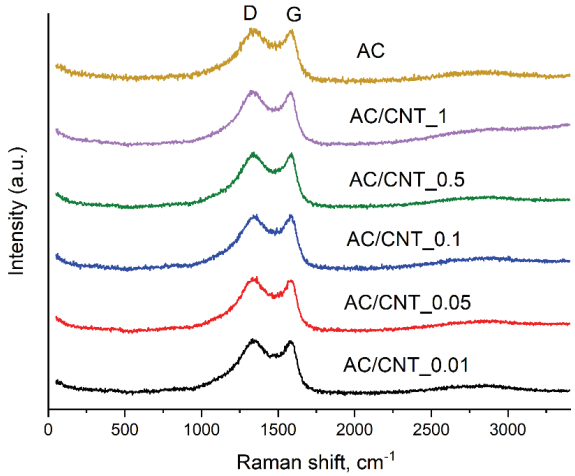

Fig. 4. Raman spectra of biochar samples

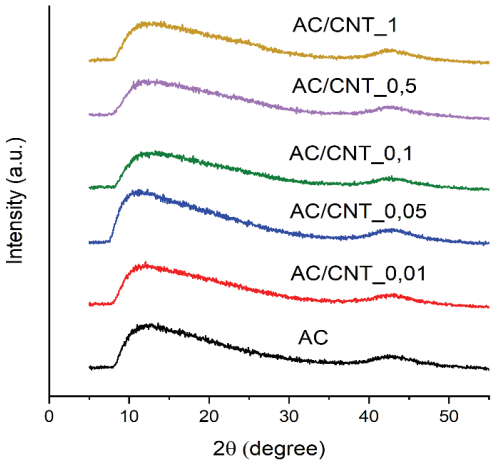

Fig. 5. XRD-patterns of biochar samples

No significant differences are observed among the Raman spectra of the analyzed samples (Fig. 4). However, calculations show that as the CNTs content increases up to 0.05 wt. %, the I_D/I_G ratio initially decreases and then increases. Notably, the sample with 1 wt. % CNTs has a slightly lower I_D/I_G ratio than the sample containing 0.5 wt. % CNTs (see Table 1).

The non-uniform trend in the defectiveness index with increasing CNTs content is likely due to differences in the composite morphology and the varying resistance of the components to alkaline treatment at high temperatures.

The X-ray diffractograms of the analyzed samples exhibit a qualitatively similar features (Fig. 5). They show a broad halo with a peak at 2θ around 12°, which is characteristic of amorphous porous carbon materials[25], and a wide peak at 2θ around 43°, which corresponds to the crystallographic plane (100) of graphite [26].

Table 1. Influence of CNTs content on the structural characteristics of the samples

Mass fraction of CNTs, wt. %	0	0.01	0.05	0.1	0.5	1
I_D/I_G	1.054	1.021	0.985	1.053	1.060	1.043
d_{100}, Å	2.114	2.111	2.101	2.111	2.117	2.101

The interplanar spacings (d_{100}), calculated using the Wulff–Bragg equation, are presented in Table 1.

It can be observed that the trend in the d_{100} values correlates with the changes in the I_D/I_G ratio. The increase in structural defects may be attributed not only to the destruction of the surface or graphene layers of the components but also to the presence of an amorphous phase within the material. Particles of this phase can potentially block pores and reduce the sorption capacity.

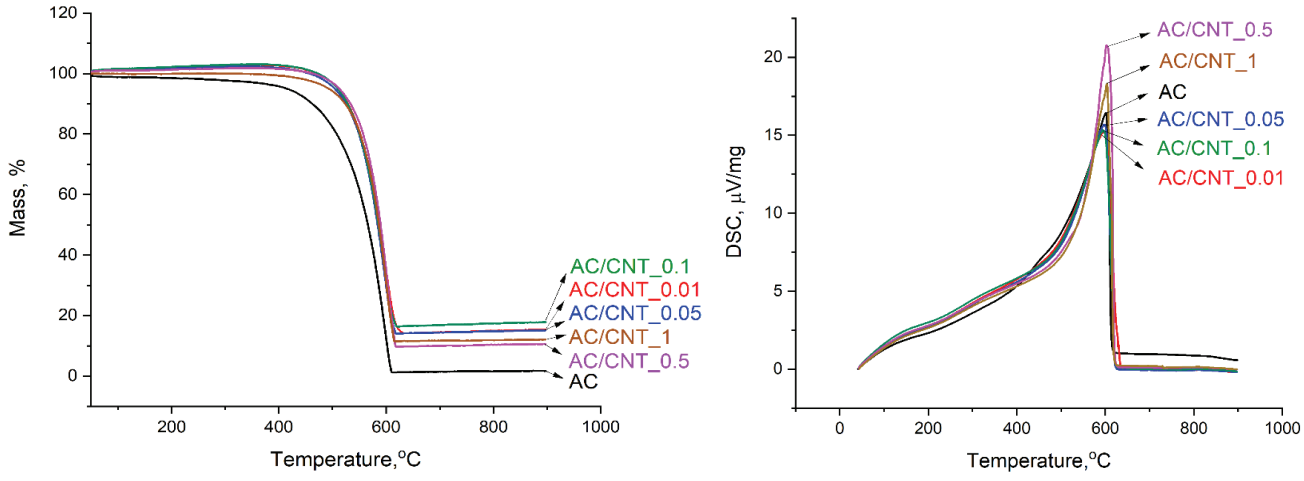

(a) *(b)*

Fig. 6. TG (*a*) and DSC (*b*) curves of biochar samples

According to thermogravimetric analysis (TGA) (Fig. 6), all samples exhibit relatively homogeneous chemical composition due to the effective decomposition of low-molecular-weight organic components and the removal of volatile functional groups during the carbonization and alkaline activation stages. The TG curves display a single prominent weight-loss region, which corresponds to a peak in the DSC curve.

The addition of CNTs contributes to a slight increase in the thermal stability of the resulting composites. However, the sample with the highest CNTs content shows the greatest initial mass loss on the TG curve compared to the other composites, likely due to its specific structural characteristics.

Particularly noteworthy is the correlation between the DSC analysis results and the data from Raman spectroscopy and X-ray diffraction. Samples that showed a decrease in structural defects (lower I_D/I_G values) also exhibited a lower exothermic effect during thermo-oxidative degradation compared to the unmodified material (without CNTs). The most intense DSC peak is observed for the sample with 0.5 wt. % CNTs, which also exhibits the highest I_D/I_G and d_{100} values.

According to the data presented in Table 2, the sample containing 0.05 wt. % CNTs demonstrates the highest specific surface area and specific micropore volume. As shown earlier, this material also has the lowest I_D/I_G and d_{100} values.

The decrease in surface area and porosity parameters with increasing defectiveness can be explained by the adverse effect of amorphous phase inclusions on the sorbent's characteristics. As the CNTs content exceeds a certain threshold, it promotes the formation of amorphous phase particles that block the pores.

Table 2. Specific surface area and specific micropore volume of the base activated carbon and composite sorbents with varying CNTs content

No.	Mass fraction of CNTs in the composite, wt. %	S_{BET}, $m^2 \cdot g^{-1}$	V_{total}, $cm^3 \cdot g^{-1}$
1	–	2945	1.703
2	0.01	2700	1.456
3	0.05	2876	1.643
4	0.1	2757	1.601
5	0.5	2690	1.570
6	1	2057	0.653

3.2. Determination of adsorption capacity

3.2.1. Comparative testing of samples under static conditions

The results of the liquid-phase adsorption studies of organic dyes on the developed materials under static conditions are presented in Fig. 7.

According to Fig. 7, the sample containing 0.05 wt. % CNTs exhibits the highest adsorption capacity, with its capacity being 25 % greater than that of the base activated carbon without CNTs. Further increases in the CNTs content do not result in a positive effect and are therefore not advisable. It is worth noting that the variation in the sorption activity of the composites toward organic dyes generally correlates with the Raman spectroscopy and X-ray diffraction data.

3.2.2. Adsorption dynamics

The experimental kinetic curves for the adsorption of MG and CR dyes under dynamic conditions are shown in Fig. 8*a*. For MG removal using the nanocomposite, equilibrium in the sorption system is reached within 30 min, while for CR it is achieved within 10 min. The studied sorbent demonstrates a high adsorption rate during the initial period (up to 10 min).

Table 3 shows the models equations used in this work to describe the mechanism of dye adsorption. Tables 4 and 5 below present the results of the mathematical analysis of the experimental data using diffusion and chemical kinetic models.

The dependence describing intraparticle diffusion (Fig. 8*b*) exhibits a multilinear curve.

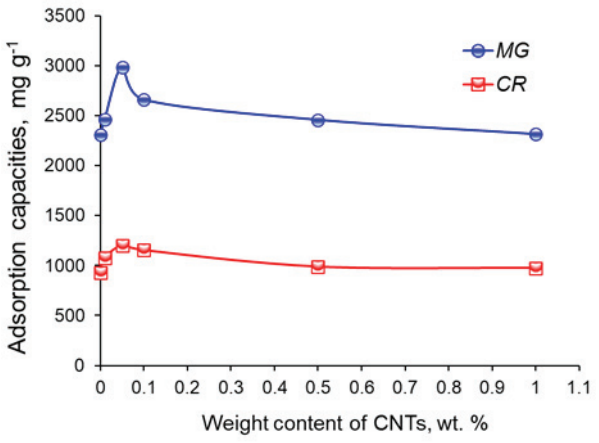

Fig. 7. Comparative adsorption capacity of peach-derived activated carbons for MG and CR dyes

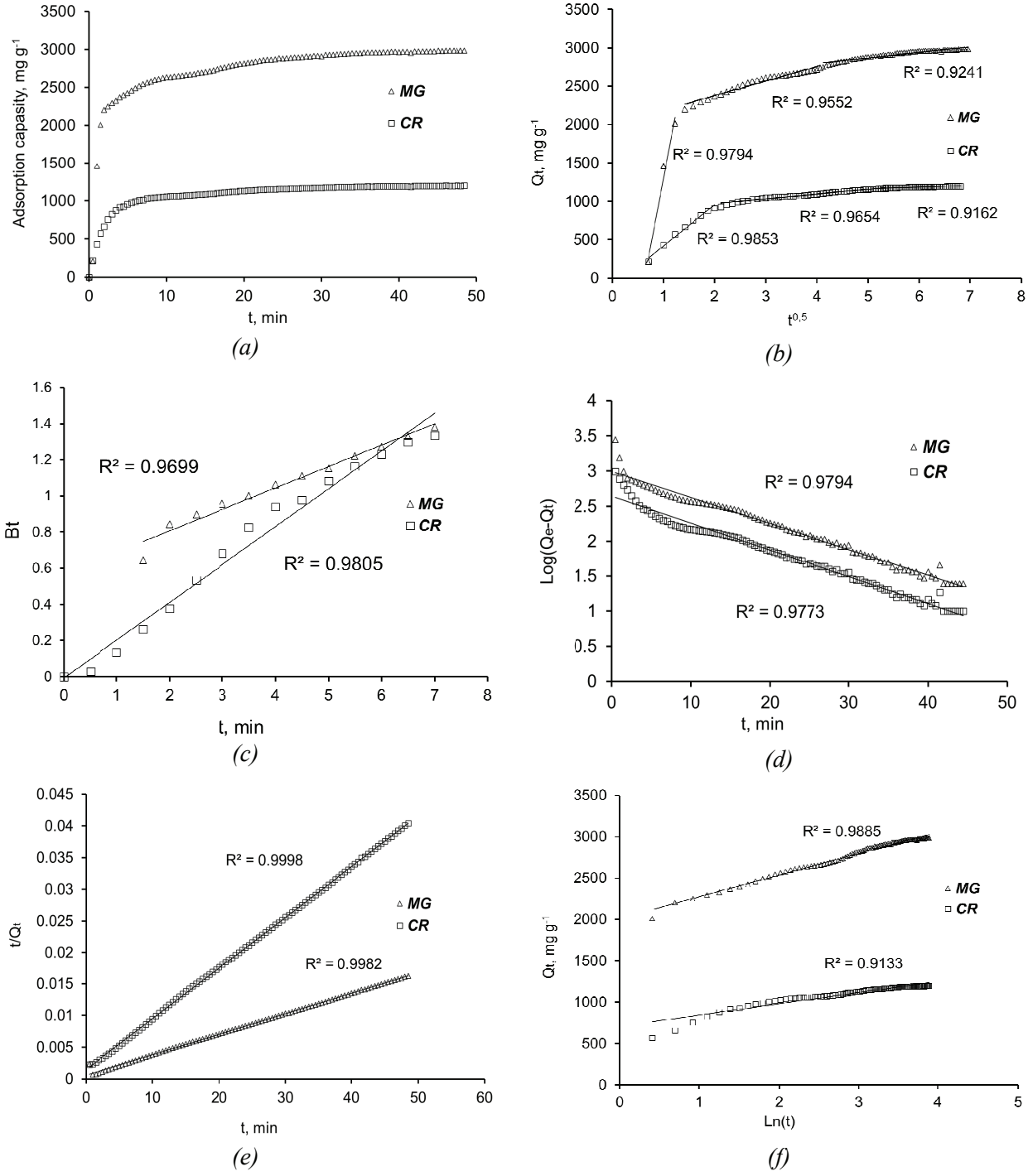

Fig. 8. Kinetic curves of MG and CR dye adsorption (*a*) and kinetic models:
b – Intraparticle diffusion; *c* – Boyd; *d* – Pseudo-first-order; *e* – Pseudo-second-order; *f* – Elovich model

Since the approximating line does not pass through the origin, there is a boundary diffusion layer effect; diffusion is not the rate-limiting step, and the diffusion process is overlapped by a surface adsorption stage [20]. These observations are characteristic for both dyes. The diffusion rate for MG is several times higher than for CR (for example, $k_{id1} = 3519.5$ mg·g^{-1}·min$^{-0.5}$ *vs.* $k_{id1} = 537.41$ mg·g^{-1}·min$^{-0.5}$). For the Boyd's model, the kinetic data were processed for $F < 0.85$, i.e., in the initial period of adsorption. The correlation of experimental data using Boyd's equation (Fig. 8*c*) further confirms the influence of intraparticle diffusion on the adsorption rate, making it possible to calculate the effective diffusion coefficient (Table 5) [27].

Table 3. Kinetic model equations* [20, 27]

Model	Equation
Pseudo-first-order model	$\lg(Q_e - Q_t) = \lg(Q_e) - \frac{k_1 t}{2.303}$
Pseudo-second-order model	$\frac{t}{Q_t} = \frac{1}{k_2 Q_e^2} + \frac{1}{Q_e} t$
Elovich model	$Q_t = \frac{1}{\beta}\ln(\alpha\beta) + \frac{1}{\beta}\ln(t)$
Intraparticle diffusion model	$Q_t = k_{id} t^{0.5} + c;$
Boyd	$F = 1 - \frac{6}{\pi^2}\sum_{n=1}^{n=\infty}\frac{1}{n^2}\exp\left(-\mathrm{Bt}\, n^2\right);$ $B = \frac{D\pi^2}{r_0^2}$

* t – adsorption time, min; Q_e – adsorption capacity at equilibrium, mg·g^{-1}; Q_t – adsorption capacity at time t, mg·g^{-1}; k_1 – rate constant for pseudo-first-order adsorption, min^{-1}; k_2 – rate constant for pseudo-second-order adsorption, g·mg^{-1}·min^{-1}; k_{id} – intraparticle diffusion coefficient, mg·g^{-1}·min$^{-0.5}$; c– boundary layer thickness (constant), mg·g^{-1}; α – initial adsorption rate, mg·g^{-1}·min^{-1}; β – desorption constant reflecting surface coverage and activation energy of chemisorption, g·mg^{-1}; F – fractional attainment of equilibrium; B – kinetic coefficient, min^{-1}; D – effective diffusion coefficient, m^2·s^{-1}; r_0 – average radius of sorbent particle, μm; Bt – dimensionless parameter.

Table 4. Parameters of chemical kinetics of dye sorption

Dies	Experimental adsorption capacity, mg g^{-1}	Pseudo-first order			Pseudo-second order			Elovich		
		Q_e, mg·g^{-1}	k_1, min^{-1}	R^2	Q_e, mg·g^{-1}	k_2, g·mg^{-1}·min^{-1}	R^2	α, mg·g^{-1}·min^{-1}	β, g·mg^{-1}	R^2
MG	2987	995.86	0.0854	0.9794	3333.3	0.00015	0.9982	532439.5	0.0038	0.9885
CR	1201	441.88	0.0884	0.9773	1250	0.00043	0.9998	22967.7	0.0074	0.9133

Table 5. Parameters of diffusion kinetic models for dye adsorption

Dies	Internal diffusion									Boyd		
	k_{id1}	k_{id2}	k_{id3}	C_1	C_2	C_3	R^2			B	$D\cdot10^{-5}$, m^{2}s^{-1}	R^2
	mg·g^{-1}·min$^{-0.5}$				mg·g^{-1}							
MG	3519.5	190.68	73.463	2213.1	1996.8	2501.6	0.9794	0.9552	0.9241	0.1184	0.004	0.9699
CR	537.41	63.574	16.722	117.4	842.07	1087.5	0.9853	0.9654	0.9162	0.2091	0.007	0.9805

If the experimental results are well approximated by the pseudo-second-order equation, the reaction between the adsorbate and functional groups occurs strictly stoichiometrically (one molecule occupies one adsorption site) [20]. For both dyes, the data show a strong correlation with this model, with $R^2 = 0.9998$ and $R^2 = 0.9982$ (Fig. 8*e*; Table 4). The rate constants are k_2 (MG) = 0.00015 g·mg^{-1}·min^{-1} and k_2 (CR) = = 0.00043 g·mg^{-1}·min^{-1}.

4. Conclusion

This study developed a method for producing an effective sorbent nanocomposite based on activated carbon derived from peach pomace, modified with carbon nanotubes. The composite material was prepared by HTC of the raw biochar with varying mass fractions of CNTs, followed by thermal treatment and alkaline activation. Characterization confirmed the presence of CNTs on the surface and within the structure of the biochar granules. The material containing 0.05 wt. % CNTs showed the most ordered carbon structure and exhibited the highest porosity among all samples. Kinetic studies under dynamic conditions determined the adsorption capacity of the nanocomposite with 0.05 wt. % CNTs for MG and CR, as well as the equilibrium sorption times: MG – 2987 $mg \cdot g^{-1}$ in 30 min, and CR – 1201 $mg \cdot g^{-1}$ in 10 min. It was established that the adsorption process for both dyes proceeds via a mixed diffusion regime, with the diffusion of MG molecules occurring 6.5 times faster than that of CR.

5. Funding

This study received no external funding.

6. Conflict of interest

The authors declare no conflict of interest.

References

1. Burakov AE, Burakova IV, Galunin EV, Kucherova AE. *New carbon nanomaterials for water purification from heavy metals*. In: Martínez LMT, Kharissova OV, Kharisov BI, editors. Handbook of Ecomaterials. Cham: Springer; 2019. p. 393-412. DOI:10.1007/978-3-319-68255-6_166

2. Goyal HB, Seal D, Saxena RC. Bio-fuels from thermochemical conversion of renewable resources: a review. *Renewable and Sustainable Energy Reviews*. 2008;12(2):504-517. DOI:10.1016/j.rser.2006.07.014

3. Guedes RE, Luna AS, Torres AR. Operating parameters for bio-oil production in biomass pyrolysis: a review. *Journal of Analytical and Applied Pyrolysis*. 2018;129:134-149. DOI:10.1016/j.jaap.2017.11.019

4. Memetova A, Tyagi I, Singh L, Karri RR, et al. Nanoporous carbon materials as a sustainable alternative for the remediation of toxic impurities and environmental contaminants: a review. *Science of the Total Environment*. 2022;838:155943. DOI:10.1016/j.scitotenv.2022.155943

5. Ali I, Babkin AV, Burakova IV, Burakov AE, et al. Fast removal of samarium ions in water on highly efficient nanocomposite based graphene oxide modified with polyhydroquinone: isotherms, kinetics, thermodynamics and desorption. *Journal of Molecular Liquids*. 2021;329:115584. DOI:10.1016/j.molliq.2021.115584

6. Bartoli M, Rosi L, Giovannelli A, Frediani P, et al. Production of bio-oils and bio-char from arundo donax through microwave assisted pyrolysis in a multimode batch reactor. *Journal of Analytical and Applied Pyrolysis*. 2016;122:479-489. DOI:10.1016/j.jaap.2016.10.016

7. Zienkiewicz-Strzalka M, Blachnio M, Derylo-Marczewska A, Winter S, et al. Mesoporous carbons and highly cross-linking polymers for removal of cationic dyes from aqueous solutions–studies on adsorption equilibrium and kinetics. *Materials*. 2024;17(6):1374. DOI:10.3390/ma17061374

8. Bushra R, Mohamad S, Alias Y, Jin Y, et al. Current approaches and methodologies to explore the perceptive adsorption mechanism of dyes on low-cost agricultural waste: a review. *Microporous and Mesoporous Materials*. 2021;319:111040. DOI:10.1016/j.micromeso.2021.111040

9. Kumar V, Sharma N, Panneerselvam B, Dasarahally Huligowda LK, et al. Lignocellulosic biomass for biochar production: a green initiative on biowaste conversion for pharmaceutical and other emerging pollutant removal. *Chemosphere*. 2024;360:142312. DOI:10.1016/j.chemosphere.2024.142312

10. Solangi NH, Kumar J, Mazari SA, Ahmed S, et al. Development of fruit waste derived bio-adsorbents for wastewater treatment: a review. *Journal of Hazardous Materials*. 2021;416:125848. DOI:10.1016/j.jhazmat.2021.125848

11. Tsai CY, Lin PY, Hsieh SL, Kirankumar R, et al. Engineered mesoporous biochar derived from rice husk for efficient removal of malachite green from wastewaters. *Bioresource Technology*. 2022;347:126749. DOI:10.1016/j.biortech.2022.126749

12. Choudhary M, Kumar R, Neogi S. Activated biochar derived from opuntia ficus-indica for the efficient adsorption of malachite green dye, Cu^{+2} and Ni^{+2} from water. *Journal of Hazardous Materials*. 2020;392:122441. DOI:10.1016/j.jhazmat.2020.122441

13. Bian Y, Zhang F, Liu Q, Mo X, et al. Simultaneous removal capacity and selectivity of Cd(ii) and Ni(II) by $KMnO_4$ modified coconut shell and peach kernel biochars. *Journal of Water Process Engineering*. 2024;65:105862. DOI:10.1016/j.jwpe.2024.105862

14. Sismanoglu S, Abdulmahdi Shakir S, Sahin Kol H, Bani Hani Y, et al. Comparison of effective removal of cationic malachite green dye from waste water with three different adsorbents: date palm, date palm biochar and phosphated biochar. *International Journal of Environmental Analytical Chemistry*. 2025;105(5):981-1000. DOI:10.1080/03067319.2023.2278084

15. Chen L, Mi B, He J, Li Y, et al. Functionalized biochars with highly-efficient malachite green adsorption property produced from banana peels via microwave-assisted pyrolysis. *Bioresource Technology*. 2023;376:128840. DOI:10.1016/j.biortech.2023.128840

16. Gamboa DMP, Abatal M, Lima E, Franseschi FA, et al. Sorption behavior of azo dye Congo red onto activated biochar from haematoxylumcampechianum waste: gradient boosting machine learning-assisted bayesian optimization for improved adsorption process. *International Journal of Molecular Sciences*. 2024;25(9): 4771. DOI:10.3390/ijms25094771

17. Liu Z, Zhang J, Zhang L, Guan Y, et al. Efficient removal of Congo red and methylene blue using biochar from medulla tetrapanacis modified by potassium carbonate. *Bioresource Technology*. 2023;376:128912. DOI:10.1016/j.biortech.2023.128912

18. Wijaya A, Yuliasari N. Biochar derived from rice husk as effective adsorbent for the removal Congo red and procion red MX-5B dyes. *Indonesian Journal of Material Research*. 2023;1(1):1-7. DOI:10.26554/ijmr.2023111

19. Burakov A, Romantsova I, Kucherova A, Tkachev A. Removal of heavy-metal ions from aqueous solutions using activated carbons: effect of adsorbent surface modification with carbon nanotubes. *Adsorption Science & Technology*. 2014;32(9):737-747. DOI:10.1260/ 0263-6174.32.9.737

20. Memetova AE, Burakova IV, Burakov AE, Memetov NR, et al. Effective adsorption of toluene and benzene on coconut activated carbon modified with carbon nanotubes: kinetics, isotherms and thermodynamics. *Adsorption*. 2023;29(5-6):335-349. DOI:10.1007/s10450-023-00405-y

21. Inyang M, Gao B, Zimmerman A, Zhou Y, et al. Sorption and cosorption of lead and sulfapyridine on carbon nanotube-modified biochars. *Environmental Science and Pollution Research*. 2015;22(3):1868-1876. DOI:10.1007/s11356-014-2740-z

22. Osman AI, Blewitt J, Abu-Dahrieh JK, Farrell C, et al. Production and characterisation of activated carbon and carbon nanotubes from potato peel waste and their application in heavy metal removal. *Environmental Science and Pollution Research*. 2019;26(36):37228-37241. DOI:10.1007/s11356-019-06594-w

23. Perumal RS, Muralidharan B. Activated biochar derived from Ricinus communis outer shell: influence of KOH impregnation ratio on physicochemical properties and EMI shielding effectiveness. *Results in Engineering*. 2025;25:104362. DOI: 10.1016/j.rineng.2025.104362

24. Kayakool FA, Pant H, Paul M, Dos Reis GS, et al. Mesoporous carbon derived from lignin sulfonate as a sustainable cathode for high-performance aluminium batteries. *Carbon Resources Conversion*. 2025;8(1):100301. DOI:10.1016/j.crcon.2024.100301

25. Badin DA, Burakov AE, Kuznetsova TS, Burakova IV, et al. Hydrocar based on sunflower meal modified with iron oxide for effective removal of lead ions from aqueous solutions: kinetics. *Perspektivnye Materialy = Inorganic Materials: Applied Research*. 2024;10:25-36. DOI:10.30791/1028-978X-2024-10-25-36 (In Russ.)

26. Memetova A, Tyagi I, Rao Karri R, Suhas, et al. High-density nanoporous carbon materials as storage material for methane: a value-added solution. *Chemical Engineering Journal*. 2022;433:134608. DOI:10.1016/ j.cej.2022.134608

27. Khim HCh, Mohd AH, Gasim H. Boyd's film diffusion model for water contaminant adsorption: Time for an upgrade? *Journal of Molecular Liquids*. 2024;409:125466. DOI:10.1016/j.molliq.2024.125466

Information about the authors / Информация об авторах

Ali H. K. Kadum, Postgraduate, Tambov State Technical University (TSTU), Tambov, Russian Federation; ORCID 0009-0003-4077-8634; e-mail: ali_strong_2010@yahoo.com

Irina V. Burakova, Cand. Sc. (Eng.), Associate Professor, TSTU, Tambov, Russian Federation; ORCID 0000-0003-0850-9365; e-mail: iris_tamb68@mail.ru

Dmitry A. Badin, Master's Degree Student, TSTU, Tambov, Russian Federation; ORCID 0009-0008-9953-3769; e-mail: badin.dima97@gmail.com

Sofya O. Rybakova, Student, TSTU, Tambov, Russian Federation; e-mail: sofyarybackova@yandex.ru

Alexey N. Timirgaliev, Master's Degree Student, TSTU, Tambov, Russian Federation; ORCID 0009-0006-5030-3677; e-mail: timirgalievas31@mail.ru

Vladimir O. Yarkin, Master's Degree Student, TSTU, Tambov, Russian Federation; ORCID 0009-0001-2185-0149; e-mail: sttstu90@gmail.com

Кадум Али Хуссейн Кадум, аспирант, Тамбовский государственный технический университет (ТГТУ), Тамбов, Российская Федерация; ORCID 0009-0003-4077-8634; e-mail: ali_strong_2010@yahoo.com

Буракова Ирина Владимировна, кандидат технических наук, доцент, ТГТУ, Тамбов, Российская Федерация; ORCID 0000-0003-0850-9365; e-mail: iris_tamb68@mail.ru

Бадин Дмитрий Александрович, магистрант, ТГТУ, Тамбов, Российская Федерация; ORCID 0009-0008-9953-3769; e-mail: badin.dima97@gmail.com

Рыбакова Софья Олеговна, студент, ТГТУ, Тамбов, Российская Федерация; e-mail: sofyarybackova@yandex.ru

Тимиргалиев Алексей Николаевич, магистрант, ТГТУ, Тамбов, Российская Федерация; ORCID 0009-0006-5030-3677; e-mail: timirgalievas31@mail.ru

Яркин Владимир Олегович, магистрант, ТГТУ, Тамбов, Российская Федерация; ORCID 0009-0001-2185-0149; e-mail: sttstu90@gmail.com

Tatyana S. Kuznetsova, Cand. Sc. (Eng.), Senior Lecturer, TSTU, Tambov, Russian Federation; ORCID 0000-0001-6508-2092; e-mail: kuznetsova-t-s@yandex.ru

Tatyana P. Dyachkova, D. Sc. (Chem.), Professor, TSTU, Tambov, Russian Federation; ORCID 0000-0002-4884-5171; e-mail: dyachkova_tp@mail.ru

Alexander E. Burakov, Cand. Sc. (Eng.), Associate Professor, TSTU, Tambov, Russian Federation; ORCID 0000-0003-4871-3504; e-mail: m-alex1983@yandex.ru

Кузнецова Татьяна Сергеевна, кандидат технических наук, старший преподаватель, ТГТУ, Тамбов, Российская Федерация; ORCID 0000-0001-6508-2092; e-mail: kuznetsova-t-s@yandex.ru

Дьячкова Татьяна Петровна, доктор химических наук, профессор, ТГТУ, Тамбов, Российская Федерация; ORCID 0000-0002-4884-5171; e-mail: dyachkova_tp@mail.ru

Бураков Александр Евгеньевич, кандидат технических наук, доцент, ТГТУ, Тамбов, Российская Федерация; ORCID 0000-0003-4871-3504; e-mail: m-alex1983@yandex.ru

Received 15 April 2025; Revised 11 May 2025; Accepted 14 May 2025

Copyright: © Kadum AHK, Burakova IV, Badin DA, Rybakova SO, Timirgaliev AN, Yarkin VO, Kuznetsova TS, Dyachkova TP, Burakov AE, 2025. This article is an open access article distributed under the terms and conditions of the Creative Commons Attribution (CC BY) license (https://creativecommons.org/licenses/by/4.0/).